Noise Generated by an Airfoil Located in the Wake of a Circular Cylinder

Man Zhang[1] and Abdelkader Frendi[2]

Abstract In this paper, a problem involving noise radiation from a bluff body is solved numerically using a hybrid RANS-LES method. In particular the problem of noise radiated by an airfoil leading edge located in the wake of a circular cylinder is addressed. Our results compare well to experimental measurements and other CFD computations. It is found that the hybrid RANS-LES method is able to resolve enough turbulent scales to compute the nearfield noise spectra and the directivity pattern. Our CFD results indicate that the coherent structures are responsible for the peak Strouhal number in the spectra.

1.1 Introduction

One of the biggest challenges facing aerospace engineers is the problem of noise pollution. As air traffic increases in coming years, the noise level in communities surrounding airports will increase leading to a deterioration of the quality of life. This has prompted the Federal Aviation Administration (FAA) to set a goal of reducing noise emission from aircrafts by 10 dB which is a very aggressive target [1]. This in turn has resulted in a renewed research effort to identify the sources of noise and to develop noise control strategies; active and/or passive.

From a computational view point, in order to identify the sources of noise, one needs to perform unsteady turbulent flow computations. In the past, these computations were carried-out using either direct numerical simulation (DNS) or large eddy simulation (LES), which are computationally intensive and not practical at high Reynolds numbers. However, in the last two decades, a new class of methods known as bridging methods have been developed. These methods take advantage of the large experiences gained in the RANS methods to bridge the gap to the LES methods [2-6] and offer a cost-effective way of resolving more scales of turbulence based on available computational resources.

[1] Graduate student, MAE Department, UAHuntsville, Huntsville, AL 35899

[2] Professor Abdelkader Frendi (✉), MAE Department, UAHuntsville, Huntsville, AL 35899. E-mail:kader.frendi@uah.edu

1.2 Mathematical Model and Method of Solution

The mathematical model is composed of the standard unsteady Reynolds Averaged Navier-Stokes equations with a two-equation eddy viscosity model based on Mentor shear stress transport model [7]. This model has been modified to accommodate a hybrid RANS-LES method (HRLES) [8-10]. The LES turbulent kinetic energy equation, k^{sgs}, is used to obtain the subgrid scale quantities

$$\frac{\partial}{\partial t}\left(\overline{\rho}k^{sgs}\right)+\frac{\partial}{\partial x_i}\left(\overline{\rho}\widetilde{u}_j k^{sgs}\right)=\overline{\rho}\tau_{ij}^{sgs}\frac{\partial\widetilde{u}_i}{\partial x_j}-C_\varepsilon\overline{\rho}\frac{\left(k^{sgs}\right)^{3/2}}{\Delta}+\frac{\partial}{\partial x_j}\left[\left(\frac{\widetilde{\mu}}{\mathrm{Pr}}+\frac{\mu^{sgs}}{\mathrm{Pr}_t}\right)\frac{\partial k^{sgs}}{\partial x_j}\right] \quad (1)$$

where

$$\mu^{sgs}=C_\nu\overline{\rho}\Delta\sqrt{k^{sgs}} \quad (2)$$

is the subgrid eddy viscosity. In the above equations, $\overline{\rho}$ is the time averaged velocity, $\widetilde{u}$ and $\widetilde{\mu}$ the mass-averaged fluid velocity and viscosity, Δ the subgrid scale filter width, $\overline{\rho}\tau_{ij}$ the unresolved stress and Pr and Pr_t are the molecular and turbulent Prandtl numbers, respectively. The coefficients C_ν and C_ε are obtained dynamically as part of the solution. The "sgs" superscript refers to subgrid scale quantity.

The hybrid RANS-LES governing equations are written in a generic from as

$$\frac{\partial}{\partial t}\left(\vec{E}\right)+\frac{\partial}{\partial x_j}\left(\widetilde{u}_j\vec{E}\right)=\frac{\partial}{\partial x_j}\left(\vec{G}_{trans}\right)+\vec{G}_{src}+\frac{\partial}{\partial x_j}\left(\vec{G}_{Ttrans}^{hybrid}\right)+\vec{G}_{Tsrc}^{hybrid} \quad (3)$$

where $\vec{E}=\left\{\overline{\rho},\overline{\rho}\widetilde{u}_j,E,\overline{\rho}k\right\}$ and the right hand side of the above equation consists of the original transport $\left(\vec{G}_{trans}\right)$ and source $\left(\vec{G}_{src}\right)$ vectors without the fluctuating turbulence terms. These later terms are written in hybrid vectors as;

$$\vec{G}_{Ttrans}^{hybrid}=F\vec{G}_{Ttrans}^{rans}+(1-F)\vec{G}_{Ttrans}^{sgs} \quad (4)$$

$$\vec{G}_{Tsrc}^{hybrid}=F\vec{G}_{Tsrc}^{rans}+(1-F)\vec{G}_{Tsrc}^{sgs}. \quad (5)$$

The blending function is defined as

$$F=\tanh(\arg_1^4) \quad (6)$$

with

$$\arg_1 = \max\left(2\frac{\sqrt{k}}{0.09\omega d}, \frac{500\bar{\nu}}{d^2\omega}\right) \tag{7}$$

where d is the distance to the wall. In the near wall region, the HRLES model becomes a RANS model using $(k-\omega)$ equations for closure [7]. Away from the wall, the HRLES model becomes an LES that uses the $k-$equation to obtain the sub-grid viscosity.

All the computational results presented in this paper are obtained using a finite volume flow solver developed at NASA Langley and known as FUN3D which stands for Fully Unstructured Navier-Stokes [11]. The code has been used extensively on a wide range of applications and its user base has grown beyond NASA Langley to include industry and academic institutions. An unstructured grid generation software known as VGRID [12] is used to generate our 3D grids. To generate an unsteady solution using FUN3D, we first obtain a steady base flow using the RANS model, then switch to the unsteady model that uses the described hybrid RANS-LES model. Five sub-iterations per time-step are used, and an optimized second-order backward differencing scheme is chosen to obtain at least two orders of magnitude reduction in the residuals of governing equations.

1.3 Results and Discussions

In order to validate our mathematical model and numerical approach we use the experimental setup given in Jacob et al. [13]. Figure 1.1 shows the geometric arrangement with all the distances given in mm. There is a 2 mm off-set in the vertical direction between the cylinder axis and the airfoil leading edge this was balanced by a 2 degree angle of attack. A conventional NACA0012 airfoil with a 100 mm cord and 12 mm thickness was used in the test and hence in our computations. The cylinder diameter is 10 mm, and the distance between the cylinder and the airfoil leading edge is also one cord length. The spanwise extent of the cylinder and airfoil is 48 mm. Air at a pressure of 98.9 kPa and temperature of 293 K is used. The flow condition used are; mean flow Mach number $M_0 = 0.21$, mean flow velocity $U_0 = 72$ m/s, Reynolds number based on cylinder diameter $\mathrm{Re}_d = 48000$. The computational domain includes all the geometric features shown on Fig. 1.1 and extends (-150, 300), (-100, 100) and (0,48) mm in the x, y and z directions, respectively. It is important to note that the leading edge of the airfoil serves as the origin of our coordinate system and therefore the cylinder center is at -105 mm in x-direction. Figure 1.2 shows a cross-section of the grid in the streamwise and vertical directions with Fig. 1.2(a) showing the grid between the

cylinder and the airfoil, Fig. 1.2(b) showing a zoomed-in view of the grid around the cylinder and Fig. 1.2(c) that around the airfoil leading edge. Our resolution is such that $y^+ < 1$ in the direction normal to solid wall and x^+ and z^+ ~ 50. These numbers are widely used in the literature and are adequate for a hybrid RANS-LES computation. Given these parameters, our overall grid was composed of 64 million cells. Grid refinement studies are not possible when using hybrid RANS-LES modelling as the space filtering operation is grid size dependent. None the less, it is critical to use a grid that captures the physics of the problem as accurately as possible. To this end, comparisons to experimental data are even more critical when using hybrid RANS-LES.

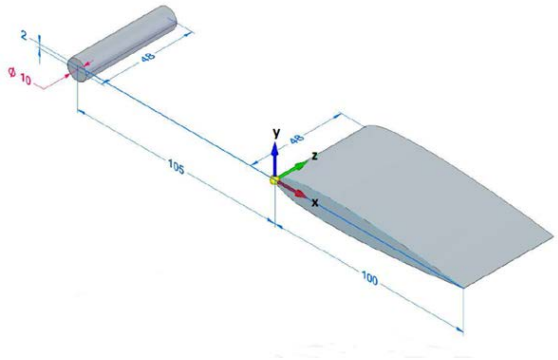

Fig. 1.1 Rod-Airfoil geometric configuration

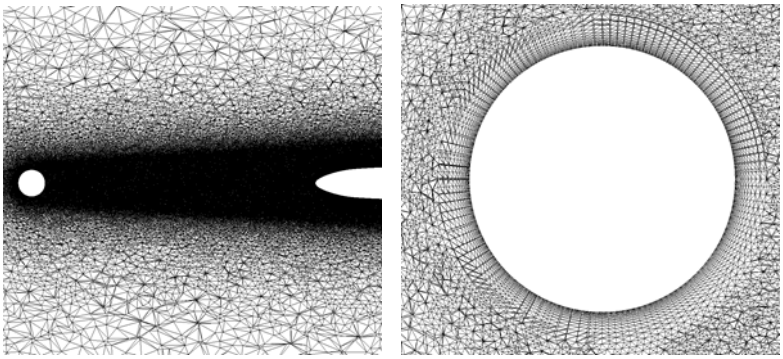

(a) **(b)**

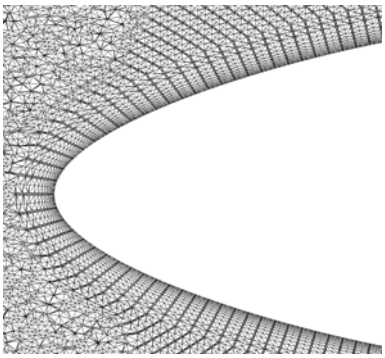

(c)

Fig. 1.2 Cross-section of the Grid Used; (a) grid between cylinder and airfoil, (b) grid around cylinder and (c) grid around airfoil

In the discussion that follows, the lengths are scaled by the cord and the velocities by U_0. In addition to comparing our results to the experimental data of Jacob et al. [13], we also compare to the CFD results of Greschner et al. [14] who used a different hybrid RANS-LES model in their computations. Figure 1.3 shows the nondimensional mean velocity profile and the nondimensional root-mean-square (rms) of the velocity fluctuations at two different nondimensional downstream locations; (a) -0.255 and (b) 0.25. Our results compare favorably to the experimental data and previous CFD results especially those of the rms velocity. It is important to point out that in the CFD solution the inlet mean flow used was uniform whereas in the experiments the mean flow was emanating from a rectangular jet which decays with downstream distance and away from the core of the jet. Both CFD results overestimate the near wall region of the mean velocity profile, Figure 1.3 (b). It is well-known that hybrid RANS-LES models tend to over predict the velocity in this region, however the RMS velocity fluctuations are well predicted by both models. In the wake region of the rod, Fig. 1.3(a), our CFD results capture the peak centreline velocity well, however the extent of the wake is over-predicted partly due to the differences between the experimental setup and the CFD input, as explained above.

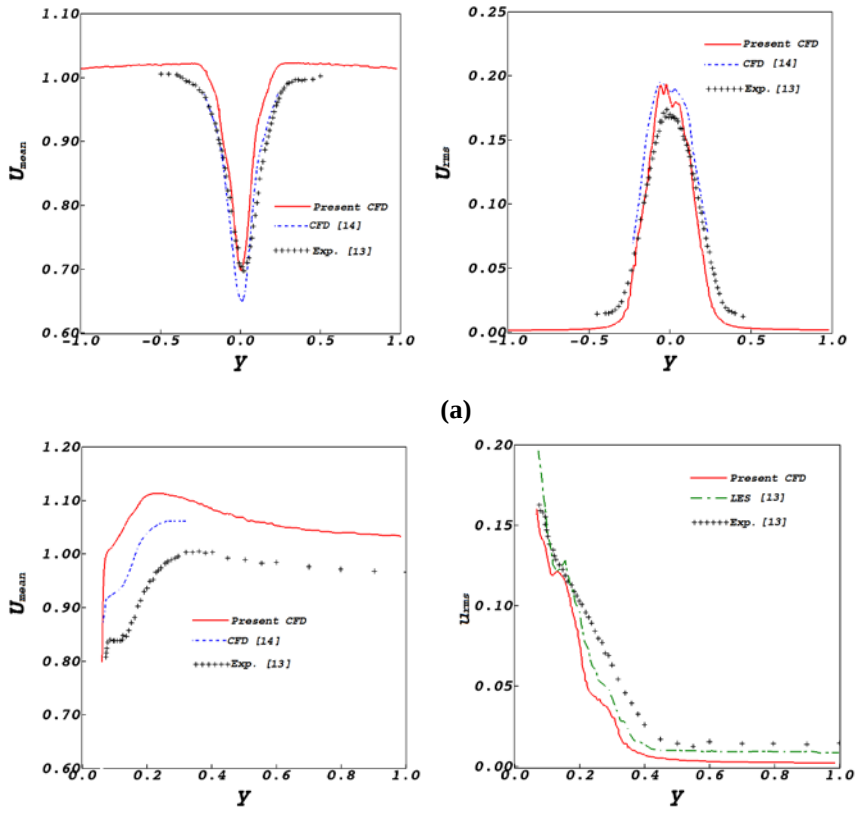

Fig. 1.3 Comparison of the mean velocity profile (left) and rms velocity fluctuation profile (right) to experimental data [13] and prior CFD results [14]. (a) x=-0.255 an (b) x=0.25

Figure 1.4 shows a comparison of the the velocity spectra at x=0.25 and y=0.08. Our results show a slight shift in the peak Strouhal number and a higher level than the experimental results at Strouhal numbers above the peak value. The shift in peak Strouhal number has been reported in the literature and attributed to the use of HRLES method.

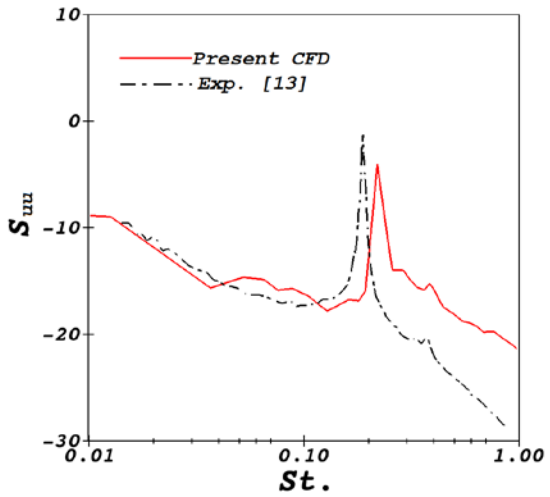

Fig. 1.4 Comparions of the predicted velocity spectra to that measured for x=0.25 and y=0.08.

Figure 1.5(a) shows the computed nearfield pressure spectrum at x=0.75 and y=0.7. Similar to the velocity spectrum, the pressure spectrum shows a peak Strouhal number of 0.24, which is in good agreement with that measured [13] in the farfield at x=0.75 and y=15.0, Fig. 1.5(b). Notice the big difference in dB-level between the two spectra because of the observer location, i.e. y-location.

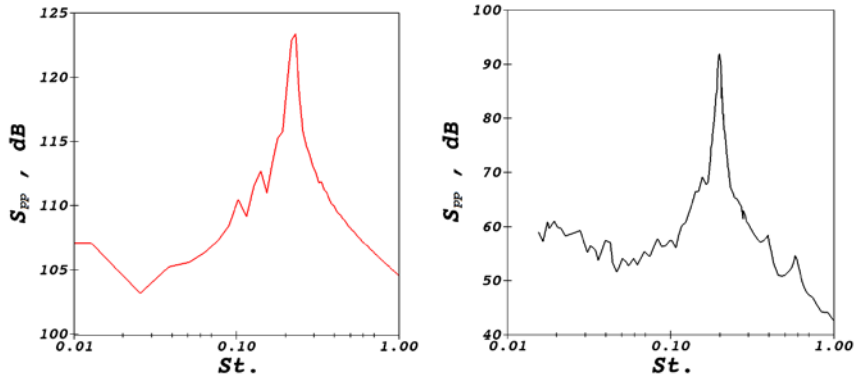

Fig. 1.5 (a) Computed nearfield pressure spectrum, x=0.75 and y=0.7; (b) measured farfield pressure spectrum [13], x=0.75 and y=15.0.

Figure 1.6 show an instantaneous Q-criterion iso-surface colored by velocity for q=0.0001. The figure shows clearly large coherent structures traveling downstream over the airfoil surface. These structures are shed at regular intervals and

are responsible for the large peak in the spectrum shown on Fig. 1.5. In addition to these large structures, smaller turbulent structures are also present on Fig. 1.6. The figure shows the ability of HRLES to capture various size turbulent strcutures.

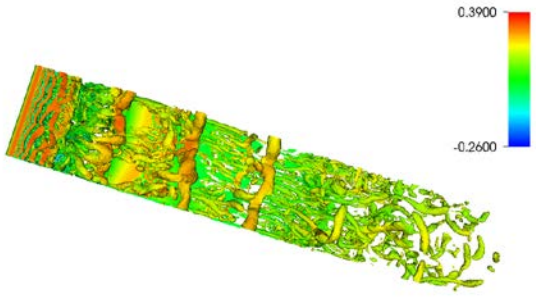

Fig. 1.6 Instantaneous Q-criterion iso-surface colored by velocity.

Figure 1.7 shows instantaneous CFD schlieren, which shows the log of the density gradient contours. The figure clearly shows the location of the coherent structures represented by the darker spots over the airfoil. This is an indication that these structures are indeed responsible for large density gradients in the flowfield and hence are the source of noise both in the nearfield and farfield.

Fig. 1.7 Instantaneous CFD schlieren showing the locus of the density gradient.

Figure 1.8 shows the noise radiation directivity around the leading, Fig. 1.8(a), and trailing, Fig. 1.8(b), edges of the airfoil on a circle of radius 0.7. Both figures show that the highest noise level is in the area near the surface and directly above and below the airfoil.

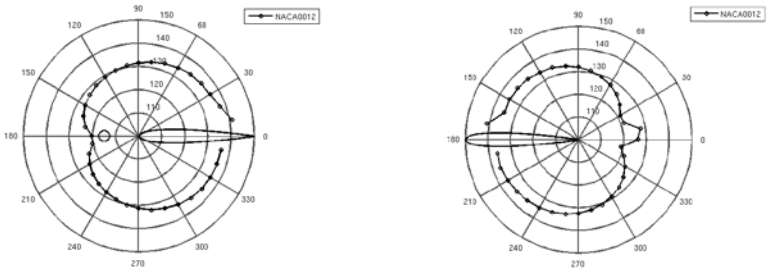

(a) **(b)**

Fig. 1.8 Noise radiation directivity around the airfoil (a) leading edge (b) trailing edge.

1.4 Conclusions

In this paper a hybrid RANS-LES method has been used to compute the noise radiated by the leading and trailing edges of a NACA0012 airfoil. Comparison of our computational results to experimental data showed good overall agreement. Our computational results show the ability of HRLES to capture turbulent structures relevant to noise radiation. Our computational results revealed that large coherent structures are responsible for the peak Strouhal number. The noise directivity is directly above and below the airfoil surface.

References

[1] NASA Aeronautics Blueprint: Toward a Bold New Era in Aviation. http://www.aerospace.nasa.gov/aero_blueprint/cover.html.

[2] Girimaji, S. S., "Partially-Averaged Navier-Stokes for Turbulence: A Reynolds Averaged Navier-Stokes to direct numerical simulation bridging method", Journal of Applied Mechanics, Vol. 73, No.3, pp. 413-421.

[3] Squires, K.D., Frosythe, J.R., and Spalart, P.R., "Detached-Eddy Simulation of the Separated Flow Around a Forebody Cross-section", Direct and Large-Eddy Simulation IV, ERCOFTAC Series, Vol. 8, Geurts, R. Friedrich and O. Metais, Editors, Kluwer Academic Press, 2001, pp. 481-500.

[4] Frendi, A., Tosh, A., Girimaji, S. "Flow Past a Backward Facing Step: Comparison of PANS, DES and URANS Results with Experiments", International Journal of Computational Methods in Engineering Science and mechanics, Vol. 8, Issue 1, pp. 23-38, 2006.
[5] Hahn, P.V., and Frendi, A. “Interaction of Three-Dimensional Protuberances with a Supersonic Turbulent Boundary Layer”, AIAA Journal, Vol. 51, No. 7, 2013, pp. 1657-1666.
[6] Peugeot J.W., and Frendi A. “Toward the understanding of Flow-Induced Vibrations in Rocket-Engine Manifold”, Journal of Propulsion and Power, Vol. 29, No. 6, 2013, pp. 1468-1477.
[7] Menter, F. R., “Two-Equation Eddy-Viscosity Turbulence Models for Engineering Applications,” AIAA Journal, Vol. 32, No. 8, 1994, pp. 1598–1605.
[8] Vatsa, V.N., and Lockard, D.P., “Assessment of hybrid RANS/LES turbulence models for aeroacoustics applications”, AIAA-2010-4001.
[9] Lynch, C.E. and Smith, M.J., “Extension and exploration of a hybrid turbulence model on unstructured grids”, AIAA Journal, Vol. 49, 2011, pp. 2585-2591.
[10] Baurle, R.A., Tam, C.J., Edwards, J.R. and Hassan H.A., “Hybrid simulation approach for cavity flows: Blending, algorithm, and boundary treatment issues”, AIAA Journal Vol. 41, 2003, pp. 1463-1480.
[11] FUN3D webpage: http://fun3d.larc.nasa.gov.
[12] VGRID webpage: http://tetruss.larc.nasa.gov/vgrid/.
[13] Jacob, M.C., Boudet, J., Casalino, D., and Michard, M., “A rod-airfoil exper iment as benchmark for broadband noise modeling Theoretical and Computational Fluid Dynamics”, Vol.19, 2005, pp. 171-196.
[14] Greschner, B., Thiel,e F., Jacob, M.C. and Casalino, D., 2008 “Prediction of sound generated by a rod-airfoil configuration using EASM DES and the generalized Lighthill/FW-H analogy”, Computers & Fluids Vol. 37, 2008, pp. 402-413.